

## Particlelike Behavior of Topological Defects in Linear Wave Packets in Photonic Graphene

Zhaoyang Zhang,<sup>1</sup> Feng Li,<sup>1,2,\*</sup> G. Malpuech,<sup>3</sup> Yiqi Zhang,<sup>1</sup> O. Bleu,<sup>3</sup> S. Koniakhin,<sup>3</sup> Changbiao Li,<sup>1</sup>  
Yanpeng Zhang,<sup>1,†</sup> Min Xiao,<sup>4,5,‡</sup> and D. D. Solnyshkov<sup>3</sup>

<sup>1</sup>Key Laboratory for Physical Electronics and Devices of the Ministry of Education & Shaanxi Key Lab of Information Photonic Technique, School of Electronic and Information Engineering, Xi'an Jiaotong University, Xi'an 710049, China

<sup>2</sup>Department of Physics and Astronomy, University of Sheffield, Sheffield S3 7RH, United Kingdom

<sup>3</sup>Institut Pascal, Université Clermont Auvergne, CNRS, SIGMA Clermont, F-63000 Clermont-Ferrand, France

<sup>4</sup>Department of Physics, University of Arkansas, Fayetteville, Arkansas 72701, USA

<sup>5</sup>National Laboratory of Solid State Microstructures and School of Physics, Nanjing University, Nanjing 210093, China



(Received 20 July 2018; revised manuscript received 8 April 2019; published 14 June 2019)

Topological defects, such as quantum vortices, determine the properties of quantum fluids. Their study has been at the center of activity in solid state and BEC communities. In parallel, the nontrivial behavior of linear wave packets with complex phase patterns was investigated by singular optics. Here, we study the formation, evolution, and interaction of optical vortices in wave packets at the Dirac point in photonic graphene. We show that while their exact behavior goes beyond the Dirac equation and requires a full account of the lattice properties, it can be still approximately described by an effective theory considering the phase singularities as “particles”. These particles are capable of mutual interaction, with their trajectory obeying the laws of dynamics.

DOI: [10.1103/PhysRevLett.122.233905](https://doi.org/10.1103/PhysRevLett.122.233905)

Topological invariants [1,2] become as important in physics as the symmetries [3]. They open a new dimension for the exploration of fundamental possibilities and the creativity of engineering. The quantum Hall effect [4–7] and topological insulators [8–10] have shown that the band structure of periodic systems is not limited to mere dispersion, and that there can be chiral edge states protected by topological invariants of the bands (e.g., Chern number [11]). The topological invariants can characterize not only such rigid structures as the bands, but also define the properties of the quantum fluids by determining the existence of topological defects [12,13]. Indeed, quantum vortices, discovered in superconductors [14], liquid helium [15,16], and Bose condensates [17], are protected by a topological invariant—their winding number [2,18]. The same topological invariant protects the phase singularities in linear (noninteracting) wave interference [19], described not only for light [20,21] but also for tidal waves [22,23].

Fluids are usually interacting [24], and quantum vortices have mostly been analyzed in interacting systems: for example, in superconductors and in Bose condensates, the vortex size is determined by the interactions [25]. Phase singularities, being just zero density points, are less limited by physical bounds: for example, their speed can exceed the speed of light [19], and there is in general no strict connection between the number of vortices and the orbital angular momentum (OAM) of a beam [26–28]. Because of this, topological defects in wave interference were seen as being objects somewhat “less real” than similar defects in

the interacting quantum fluids. The distinction between the interacting and noninteracting case has become a matter of debate [29,30], because in many works vortices were used as a smoking gun of superfluidity [31,32].

Linear optical wave packets are an important field on their own. The famous self-accelerated Airy beams [33,34] are one example, but there are also self-repairing Bessel beams [35–37], useful for optical tweezers. Even the physics of Gaussian wave packets in nontrivial systems with diabolical points, such as the honeycomb lattices widely used in topological photonics [38], has been attracting attention since a very long time, with original phenomena such as the conical refraction, predicted [39] and observed [40] a long time ago. A finalized theory describing the intensity evolution in such wave packets was developed only recently [41,42]. The phase properties of conical diffraction are understood even less. Recently, the conversion of pseudospin into OAM has been described for such wave packets at the Dirac point [43]: a vortex has been shown to appear in the center of the wave packet in the effective field of the Dirac Hamiltonian. Another work has shown the formation of several vortices in photonic Lieb lattices [44], but their dynamical behavior has not been analyzed. These works did not discuss how exactly a vortex appears in a beam with initial zero OAM, if the winding number is a topological invariant that cannot be changed smoothly. Such questions belong to the field of singular optics of linear and nonlinear media [45,46] and lattices [47].

In this Letter, we realize photonic graphene in a new atomic vapor system for the first time, which allows us to tune *in situ* the potential of the optically induced lattices by precisely varying the frequency detuning, thus enabling us to study the dynamic evolution of the topological defects and settle the above issues positively. We find that optical vortices in linear wave packets exhibit many features typical for topological defects in nonlinear quantum fluids. Their trajectories obey the laws of dynamics: in particular, we observe the effect of the Magnus force and the mutual interaction of two vortices. Finally, we show that certain features of wave packets even in the immediate vicinity of the Dirac point in graphene cannot be described by the Dirac equation, because the two pseudospin components actually coexist in the same real space.

We study the evolution of a probe beam in a honeycomb lattice (photonic graphene). The transverse beam profile can be found by looking for the solution of the wave equation in the form  $\mathbf{E}(x, y, z, t) = \mathbf{E}_0 a(x, y, z) e^{i(k_0 n z - \omega t)}$ , where  $\omega$  is the frequency of the laser beam,  $n$  is the refraction coefficient,  $k_0$  is the wave vector of light in the vacuum,  $\mathbf{E}_0$  is the amplitude, and  $a$  determines the spatial intensity distribution. The paraxial approximation  $\partial^2 a / \partial z^2 \ll k_0 \partial a / \partial z$  allows rewriting the equation as

$$i \frac{\partial a}{\partial z} = -\frac{1}{2k_0 n_0} \Delta a - k_0^2 (n^2 - n_0^2) a, \quad (1)$$

which is equivalent to the Schrödinger equation with  $z$  mapped to  $t$ , the mass  $m = \hbar k_0 n_0 / c$  ( $n_0$  is the background refraction index,  $c$  is the speed of light), and the potential  $U(x, y) = -\hbar c k_0^2 (n^2 - n_0^2)$  is determined by the variation of the refractive index. In the vicinity of the Dirac point the behavior of the wave packets is supposed to obey the Dirac equation:

$$i \hbar \frac{\partial \psi}{\partial t} = \hbar c' \mathbf{k} \cdot \boldsymbol{\sigma} \psi \quad (2)$$

written in the simplest form, where  $\psi = (\psi_A, \psi_B)^T$  is a spinor wave function with two components (in the case of graphene, these are the wave functions on the two sites of the unit cell  $A$  and  $B$ ), and  $c'$  is the effective speed of light determined by the microscopic Hamiltonian (e.g., Fermi velocity). Note that the full solution  $a(x, y, z)$  of Eq. (1) also includes a plane wave of the  $K$  point [48].

The photonic graphene is formed in a  $^{85}\text{Rb}$  vapor cell by electromagnetically induced transparency (EIT) [53], as illustrated in Fig. 1. Generally, the susceptibility experienced by a probe field  $\mathbf{E}_1$  in the  $\Lambda$ -type three-level  $^{85}\text{Rb}$  atomic configuration [Fig. 1(e)] under the effect of a coupling field  $\mathbf{E}_2$  reads [54,55]

$$\chi = \frac{iN|\mu_{31}|^2}{\hbar\epsilon_0} \times \frac{1}{(\Gamma_{31} + i\Delta_1) + \frac{|\Omega_2|^2}{\Gamma_{32} + i(\Delta_1 - \Delta_2)}} \quad (3)$$

where  $\epsilon_0$  is the vacuum dielectric constant;  $\Gamma_{31}$  (respectively,  $\Gamma_{32}$ ) is the decay rate between states  $|1\rangle$  (respectively,  $|2\rangle$ ) and  $|3\rangle$ ;  $N$  is the atomic density at  $|1\rangle$ .  $\Delta_1$  (respectively,  $\Delta_2$ ) is the frequency detuning between the atomic resonance  $|1\rangle$  to  $|3\rangle$  (respectively,  $|2\rangle$  to  $|3\rangle$ ) and the probe (respectively, coupling) field frequency, as labeled in Fig. 1(e).  $\Omega_2$  is the Rabi frequency induced by the coupling field  $\mathbf{E}_2$  and  $\mu_{31}$  is the dipole moment between levels  $|1\rangle$  and  $|3\rangle$ . The coupling field is constructed by the interference of three laser beams which induces a honeycomblike susceptibility distribution [56] with a negligibly small imaginary part [48]. The probe field is also structured to form periodical vertical fringes by two-beam interference [48] to allow selective coverage of only one set (either  $A$  or  $B$ ) of the sublattices [Figs. 1(c), 1(g)–1(i)], and to excite the  $K$  or  $K'$  valley in the momentum space [43]. In our experiment, the probe can be either Gaussian or Gauss-Laguerre with nonzero OAM. After the Rb cell, the two probe beams separate in space [Fig. 1(a)]. We record their interference with a Gaussian reference beam on a charge coupled device camera. The massless Dirac Eq. (2) is characterized by a single parameter  $c'$ . Therefore, changing this parameter is equivalent to changing the units of time. In the experiment,

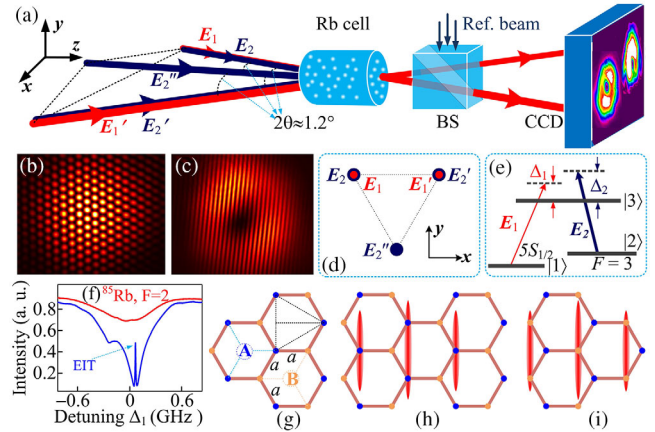


FIG. 1. (a) Experimental setup.  $\mathbf{E}_2$ ,  $\mathbf{E}'_2$ , and  $\mathbf{E}''_2$  are three coupling beams interfering to form a hexagonal optical lattice inside the rubidium vapor cell, which results in a honeycomb lattice for susceptibility due to the EIT effect.  $\mathbf{E}_1$  and  $\mathbf{E}'_1$  are two probe beams from the same laser that construct a probe field featured by equally spaced vertical fringes. BS: 50/50 beam splitter, CCD: charge coupled device camera. (b) The observed hexagonal coupling lattice. (c) The interference fringes formed by the two probe beams, both of which are set to carry an OAM = 1. (d) Spatial beam arrangement (before entering the cell) of the probe and coupling beams in the  $XY$  plane. (e) The  $\Lambda$  three-level structure coupled by the probe and coupling fields. (f) The observed absorption (upper red curve, corresponding to the transition  $^{85}\text{Rb}$ ,  $F = 2 \rightarrow F'$ ) and EIT spectra (lower blue curve) versus the probe-field detuning. (g) The schematic for the generated hexagonal lattice. (h) and (i) The beam arrangements of the periodic probe field and the induced honeycomb lattice inside the medium for exciting  $A$  and  $B$  sublattices, respectively.

varying the detuning  $\Delta_1$  changes the susceptibility of the honeycomblike atomic lattice [Eq. (3)], which changes the amplitude of the potential and the tunneling probability between the lattice sites, and thus the effective units of time (see the Supplemental Material [48]).

The nontrivial behavior of wave packets in the Dirac equation has been in the focus of theoretical studies for a long time [57], and several corresponding experiments have also appeared recently [43]. Different representations (centered on Berry curvature [58,59] or on the effective field [43]) lead to the same conclusion: wave packets in the Dirac equation are almost always associated with a nonzero OAM [58], which can be seen (and observed experimentally) as a quantum vortex.

We begin with a simple case with zero OAM of the initial wave function  $\psi_A = \exp(-r^2/2w^2)$ . The Hamiltonian [Eq. (2)] converts  $\psi_A$  to  $\psi_B$ , but because of its dependence on the polar angle of  $\mathbf{k}$ , the resulting conical refraction is accompanied by the change of winding:  $l_B = l_A \pm 1$ . Figure 2 shows the calculated images of the evolution of a Gaussian wave packet in the Dirac equation, exhibiting conical refraction:  $|\psi_A|^2$  in panels (a) and (d),  $|\psi_B|^2$  in (b) and (e), and the interference of their superposition with a reference beam in (c) and (f). The phases  $\arg(\psi_A)$  and  $\arg(\psi_B)$  do not change with time: the phase singularity is always present only in the center of  $\psi_B$ . In experiment, the emission is detected far from the Rubidium cell, and individual sites cannot be distinguished. Therefore, the total emission detected is a *superposition* of  $\psi_A$  and  $\psi_B$ , with the phase being that of a superposition of two complex fields. The position of the vortex core is therefore given by the solution of the equation  $\psi_A + \psi_B = 0$ . In an ideal Dirac picture, this condition is fulfilled along the real space direction ( $-x$  in Fig. 2), where  $\psi_A$  and  $\psi_B$  are in antiphase. The vortex core motion versus time toward the center of the excitation spot is linked with the growth of the  $\psi_B$  amplitude along this axis. The period of the full component conversion is  $T = w/c$ , but we are interested in the dynamics until the formation of a conical refraction ring at  $t = T/4$ , which

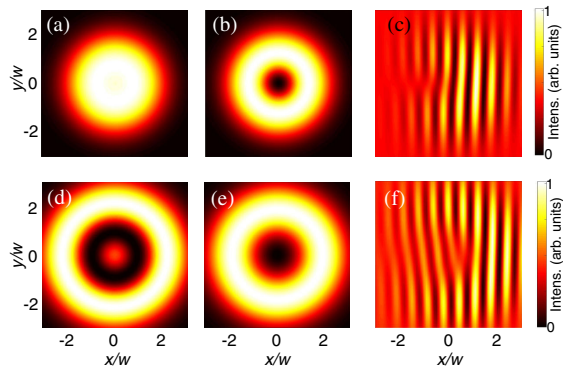


FIG. 2. Wave packet in the Dirac equation. The two rows correspond to  $4t/T = 0.67$  (1.17). Intensity: (a), (d)  $|\psi_A|^2$ , (b), (e)  $|\psi_B|^2$ . Interference: (c), (f)  $|\psi_A + \psi_B + e^{ik_r r}|^2$ ,  $k_r w = 15$ .

allows writing an approximate solution along  $x$ :  $\psi_A(x, t) = A(t)e^{-x^2/2w^2}$ ,  $\psi_B(x, t) = B(t)xctw^{-2}e^{-x^2/2w^2}$ , where  $A(t) = \cos \omega t$  and  $B(t) = \sin \omega t$  ( $\omega = 2\pi/T$ ). The equation for the vortex position reads  $A(t) + B(t)x_0ct/w^2 = 0$ , which allows us to find  $x_0(t)$ :

$$|x_0(t)| = \frac{w^2 \cot \omega t}{ct} \quad (4)$$

Figures 3(a) and 3(c) show the experimental images of the interference of the transmitted beam with a reference beam at two detunings corresponding to two different times (see movies in the Supplemental Material [48]). The vortex position is visible as a forklike dislocation (white circle), and its shift is marked by a black arrow. The experimental images were rotated to match the coordinates of Eq. (2). Panels (b) and (d) show the extracted phase. The extracted distance  $r = \sqrt{x^2 + y^2}$  from the center for the vortex (with the error bars determined by the interference fringes) as a function of time is compared in Fig. 3(e) with the analytical solution Eq. (4) (red curve,  $r(t) = |x_0(t)|$  since  $y_0 = 0$ ). The good quality of the fit confirms the interpretation (the origin of the experimental time axis is the only fitting parameter). In the analytical solution, a vortex appears at infinity and

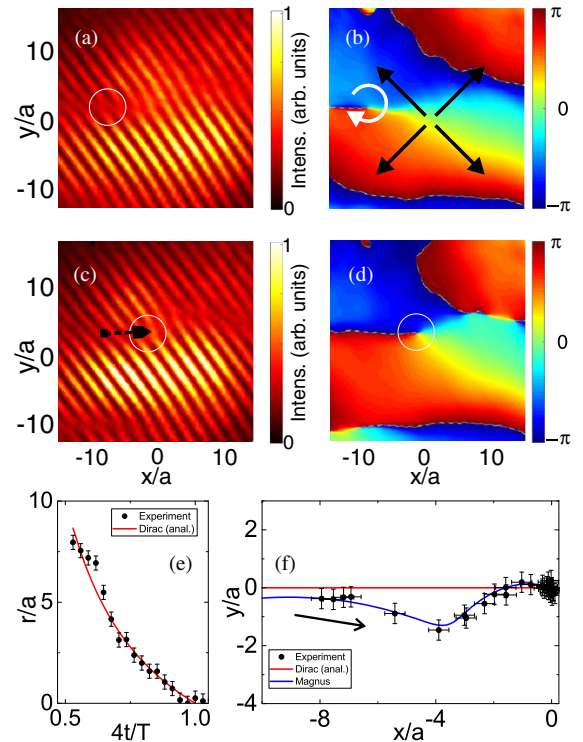


FIG. 3. Wave packet evolution. The first two rows correspond to  $\Delta_1 = 45$  (56) MHz. (a), (c) the interference pattern with a reference beam; (b), (d) extracted phase [arrows in panel (b) show different contributions to the current]. The last row shows the vortex trajectory (e)  $r(t)$  [black dots—experiment, red line—Eq. (4)] and (f)  $y(x)$  [same as (e) + blue line—Eq. (5)].

approaches the system center very rapidly in the initial moments. In the experiment, it appears as a part of a vortex-antivortex pair at a finite distance, determined by the sensitivity of the detector and the finite size of the photonic graphene lattice (see the Supplemental Material [48]).

However, the periodic modulations visible in Fig. 3(e) and the exact cycloidal experimental  $XY$  trajectory of the vortex [Fig. 3(f), black dots] cannot be simulated with the Dirac equation and Eq. (4), but can be reproduced only if one takes into account the Magnus force [60,61]  $\mathbf{F} = I\hbar(\mathbf{L} \times \mathbf{v})$ , where  $I$  is the force strength,  $\mathbf{L}$  is the vortex winding, and  $\mathbf{v}$  is the vortex velocity. The Magnus force was used to detect a single vortex in superfluid helium for the first time [62]; here we use it to prove the “reality” of the phase singularity and of the associated rotation in a two-component light beam. Considering this force as a correction [48], we find the trajectory from

$$\begin{aligned} v_x &= \eta v_x^{(0)} \cos \Omega t + v_x^{(0)}, \\ v_y &= -\eta v_x^{(0)} \sin \Omega t, \end{aligned} \quad (5)$$

where  $v_x^{(0)} = \dot{x}_0$  from Eq. (4),  $\Omega \approx 9.5\omega$  is the “cyclotron frequency” due to the Magnus force (fitting parameter), and  $\eta \approx 0.5$  characterizes the initial excitation of  $A$  and  $B$  sites determining the type of the cycloid (second fitting parameter). This trajectory is plotted in Fig. 3(f)(red curve). The microscopic mechanism is typical for the Magnus force in classical and quantum fluids [63,64]. In experiment and in full numerical simulations, the singularity is located at the center of the vortex [Figs. 3(b) and 3(d)]. Therefore, the overall outward flow due to the intensity gradient [Fig. 3(b), black arrows] is increased on one side of the singularity because of the rotating current (white arrow), creating a pressure gradient shifting the vortex laterally.

We have also studied the evolution of wave packets with nonzero OAM. The conversion of the component  $\psi_A$  into  $\psi_B$  by the Dirac Hamiltonian [Eq. (2)] changes the OAM by 1:  $l_B = l_A - 1$ . If the injected wave packet has a positive OAM  $l_A = 1$ , then the other component has  $l_B = 0$ , and the overall interference pattern shows a vortex and an antivortex canceling each other at  $t = T/4$ . In the other case, when  $l_A = -1$ ,  $l_B = -2$ , and the overall pattern shows  $L = -2$  at  $T/4$ . Here, we use the full numerical treatment in the paraxial approximation, beyond the Dirac equation. Figure 4 shows the experimental and theoretical images for a wave packet with  $L = +1$ . Panels (a,d) show the experimental interference patterns, with vortices marked by ellipses. In panel (d), two opposite vortices meet and annihilate (dashed ellipse). This is confirmed by the phase images [(b) two dislocations, (e) no dislocation]. The trajectories of the two vortices in panel (c) are well reproduced by theoretical modeling (f) (see also the Supplemental Material [48]) [fitting parameter—initial position of the vortex  $(-0.2, -0.5)a$ ].

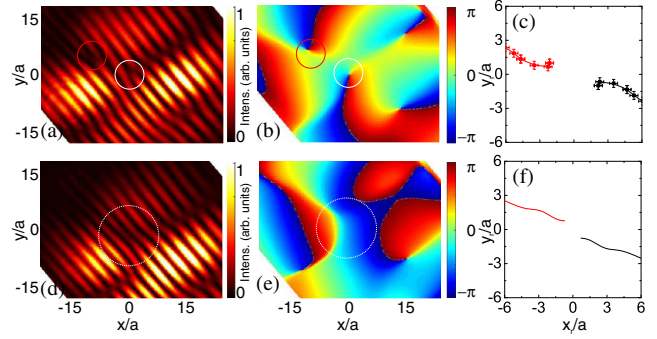


FIG. 4. Evolution of  $L = +1$ -wave packet. The two rows correspond to  $\Delta_1 = 80.4$  (96.4) MHz. Experiment: (a), (d) interference pattern, (b), (e) extracted phase. Vortex trajectories: (c) experiment (curves are guides for the eyes), (f) theory.

Figure 5 demonstrates the evolution of a wave packet with  $L = -1$  (movie in the Supplemental Material [48]). In this case, two vortices of the same sign appear in the experimental interference patterns (a), (d) and phase (b), (e). As in the case  $L = 0$ , it is possible to find an analytical solution for the vortex trajectory from the condition  $\psi_A = -\psi_B$  (see the Supplemental Material [48]), but it is again a straight line. However, in reality, each of the two vortices creates a velocity field which affects the other, leading to their mutual rotation around their center of mass [45,65], as can be seen from the experiment (c) and full numerical simulations (f) [fitting parameter—initial position of the vortex  $(-0.46, -1.8)a$ ].

Neither the cycloidal motion visible in Fig. 3(f), nor the mutual rotation seen in Figs. 5(c) and 5(f) can be reproduced with the Dirac Hamiltonian [Eq. (2)], because it neglects the fact that the two components  $\psi_A$  and  $\psi_B$  actually coexist in the same space, occupying different points. This is a fundamental limitation of the Dirac equation restricting its validity. While the wave packet

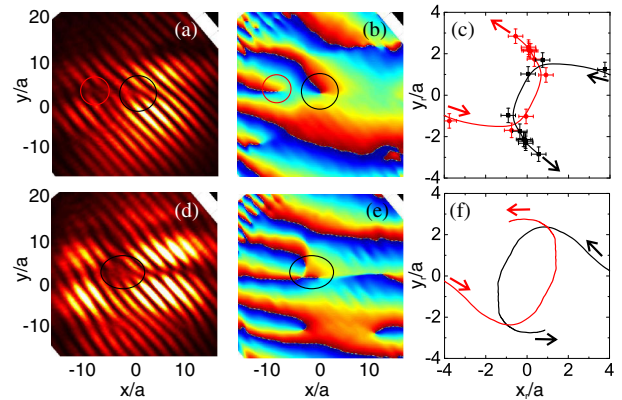


FIG. 5. Evolution of  $L = -1$ -wave packet. The two rows correspond to  $\Delta_1 = 50$  (59.6) MHz. Experiment: (a), (d) interference patterns, (b), (e) extracted phase. Trajectories of the vortices: (c) experiment (smooth curves are guides for the eyes), (f) theory.

as a whole involves wave vectors close to the Dirac point, determining the position of the vortex core with a high precision involves wave vectors much further from this point, due to the Heisenberg uncertainty principle. Both effects stem from the rotating current associated with vortices. The advantage of our configuration is that it allowed us to evidence the consequences of this current for the phase singularities themselves. The study of the dynamics of vortices is important for future applications, such as vortex memories [66,67] and gyroscopes [68,69].

To conclude, we have studied both experimentally and theoretically the behavior of OAM wave packets in photonic graphene, showing that phase singularities in linear wave packets can behave as vortices in quantum fluids, exhibiting the effects of the Magnus force and demonstrating mutual interaction. We also point out the limitations of the Dirac equation for the description of the systems with pseudospin defined in real space.

This Letter was supported by National Key R&D Program of China (Grants No. 2018YFA0307500, No. 2017YFA0303703), National Natural Science Foundation of China (Grants No. 61605154, No. 11474228, and No. 11804267), Natural Science Foundation of Shaanxi Province (Grants No. 2017JQ6039, No. 2017JZ019, No. 2018JQ6041, and No. 2016JM6029), China Postdoctoral Science Foundation (Grants No. 2016M600776, No. 2016M600777, and No. 2017T100734), and Postdoctoral Science Foundation of Shaanxi Province (Grants No. 2017BSHYDZZ54 and No. 2017BSHTDZZ18). We acknowledge the support of the project “Quantum Fluids of Light” (Grant No. ANR-16-CE30-0021), of the ANR Labex Ganex (Grant No. ANR-11-LABX-0014), and of the ANR Labex IMobS3 (Grant No. ANR-10-LABX-16-01), of the I-Site “Cap2025” (Grant No. 16-IDEX-0001). D. D. S. acknowledges the support of IUF (Institut Universitaire de France).

---

\*Corresponding author.  
felix831204@xjtu.edu.cn  
†ypzhang@xjtu.edu.cn  
‡mxiao@uark.edu

- [1] Scientific Background: Topological Phase Transitions and Topological Phases of Matter, The Nobel Prize in Physics 2016, Nobelprize.org (2016).
- [2] D. J. Thouless, *Topological Quantum Numbers in Non-relativistic Physics* (World Scientific, Singapore, 1998).
- [3] D. J. Gross, *Proc. Natl. Acad. Sci. U.S.A.* **93**, 14256 (1996).
- [4] K. V. Klitzing, G. Dorda, and M. Pepper, *Phys. Rev. Lett.* **45**, 494 (1980).
- [5] D. J. Thouless, M. Kohmoto, M. P. Nightingale, and M. den Nijs, *Phys. Rev. Lett.* **49**, 405 (1982).
- [6] M. Kohmoto, *Ann. Phys. (N.Y.)* **160**, 343 (1985).
- [7] Y. Hatsugai, *Phys. Rev. Lett.* **71**, 3697 (1993).
- [8] C. L. Kane and E. J. Mele, *Phys. Rev. Lett.* **95**, 146802 (2005).
- [9] C. L. Kane and E. J. Mele, *Phys. Rev. Lett.* **95**, 226801 (2005).
- [10] M. Z. Hasan and C. L. Kane, *Rev. Mod. Phys.* **82**, 3045 (2010).
- [11] S. S. Chern, *Ann. Math.* **47**, 85 (1946).
- [12] J. M. Kosterlitz and D. J. Thouless, *J. Phys. C* **5**, L124 (1972).
- [13] V. L. Berezinskii, *Zh. Eksp. Teor. Fiz.* **61**, 1144 (1972) [*Sov. Phys. JETP* **34**, 610 (1972)].
- [14] A. Abrikosov, *J. Phys. Chem. Solids.* **2**, 199 (1957).
- [15] L. Onsager, *Il Nuovo Cimento* **6**, 279 (1949).
- [16] R. P. Feynman and M. Cohen, *Phys. Rev.* **102**, 1189 (1956).
- [17] J. R. Abo-Shaeer, C. Raman, J. M. Vogels, and W. Ketterle, *Science* **292**, 476 (2001).
- [18] B. O’Neill, *Elementary Differential Geometry* (Academic Press, New York, 1967).
- [19] J. F. Nye and M. V. Berry, *Proc. R. Soc. A* **336**, 165 (1974).
- [20] W. Braunbek and G. Laukien, *Optik (Stuttgart)* **9**, 174 (1952).
- [21] M. R. Dennis, K. O’Holleran, and M. J. Padgett, in *Progress in Optics*, edited by E. Wolf (Elsevier, New York, 2009), Vol. 53, pp. 293–363.
- [22] W. Whewell, *Phil. Trans. R. Soc. London* **123**, 147 (1833).
- [23] M. V. Berry, *Nature (London)* **403**, 21 (2000).
- [24] L. D. Landau and E. M. Lifshitz, *Fluid Mechanics* (Pergamon Press, Oxford, 1987).
- [25] A. Leggett, *Quantum Liquids* (Oxford Graduate Texts, 2006).
- [26] M. S. Soskin, V. N. Gorshkov, M. V. Vasnetsov, J. T. Malos, and N. R. Heckenberg, *Phys. Rev. A* **56**, 4064 (1997).
- [27] G. Molina-Terriza, J. Recolons, and L. Torner, *Opt. Lett.* **25**, 1135 (2000).
- [28] M. V. Berry, *J. Opt. A* **11**, 094001 (2009).
- [29] P. Cilibrizzi, H. Ohadi, T. Ostatnický, A. Askitopoulos, W. Langbein, and P. Lagoudakis, *Phys. Rev. Lett.* **113**, 103901 (2014).
- [30] A. Amo, J. Bloch, A. Bramati, I. Carusotto, C. Ciuti, B. Deveaud, E. Giacobino, G. Grosso, A. Kamchatnov, G. Malpuech *et al.*, *Phys. Rev. Lett.* **115**, 089401 (2015).
- [31] M. W. Zwiernik, J. R. Abo-Shaeer, A. Schirotzek, C. H. Schunck, and W. Ketterle, *Nature (London)* **435**, 1047 (2005).
- [32] K. G. Lagoudakis, M. Wouters, M. Richard, A. Baas, I. Carusotto, R. Andre, L. S. Dang, and B. Deveaud-Pledran, *Nat. Phys.* **4**, 706 (2008).
- [33] M. V. Berry and N. L. Balazs, *Am. J. Phys.* **47**, 264 (1979).
- [34] G. A. Siviloglou, J. Broky, A. Dogariu, and D. N. Christodoulides, *Phys. Rev. Lett.* **99**, 213901 (2007).
- [35] J. Durmin, J. J. Miceli, and J. H. Eberly, *Phys. Rev. Lett.* **58**, 1499 (1987).
- [36] Z. Bouchal, J. Wagner, and M. Chlup, *Opt. Commun.* **151**, 207 (1998).
- [37] V. Garcés-Chaves, D. McGloin, H. Melville, W. Sibbett, and K. Dholakia, *Nature (London)* **419**, 145 (2002).
- [38] M. Rechtsman, J. Zeuner, Y. Plotnik, Y. Lumer, D. Podolsky, F. Dreisow, S. Nolte, M. Segev, and A. Szameit, *Nature (London)* **496**, 196 (2013).
- [39] W. R. Hamilton, *Trans. R. Irish Acad.* **17**, 1 (1837).
- [40] H. Lloyd, *Philos. Mag.* **1**, 112 (1833).

- [41] A. M. Belskii and A. P. Khapalyuk, *Opt. Spectrosc.* **44**, 436 (1978).
- [42] M. V. Berry, M. R. Jeffrey, and J. G. Lunney, *Proc. R. Soc. A* **462**, 1629 (2006).
- [43] D. Song, V. Paltoglou, S. Liu, Y. Zhu, D. Gallardo, L. Tang, J. Xu, M. Ablowitz, N. K. Efremidis, and Z. Chen, *Nat. Commun.* **6**, 6272 (2015).
- [44] F. Diebel, D. Leykam, S. Kroesen, C. Denz, and A. S. Desyatnikov, *Phys. Rev. Lett.* **116**, 183902 (2016).
- [45] D. Rozas, C. T. Law, and G. A. Swartzlander, *J. Opt. Soc. Am. B* **14**, 3054 (1997).
- [46] Y. V. Izdebskaya, A. S. Desyatnikov, G. Assanto, and Y. S. Kivshar, *Opt. Express* **19**, 21457 (2011).
- [47] A. Bezryadina, D. N. Neshev, A. S. Desyatnikov, J. Young, Z. Chen, and Y. S. Kivshar, *Opt. Express* **14**, 8317 (2006).
- [48] See Supplemental Material at <http://link.aps.org/supplemental/10.1103/PhysRevLett.122.233905> for the details of the experiments, simulations and calculations given in the main text and the description of the video files, which includes references [49–52].
- [49] L. Pitaevskii and S. Stringari, *Bose-Einstein Condensation*, Oxford Science Publications—International Series of Monographs on Physics 116, (Clarendon Press, Oxford, 2003).
- [50] M. Schonberg, *Il Nuovo Cimento* **12**, 103 (1954).
- [51] L. D. Landau and E. M. Lifshitz, *The Classical Theory of Fields* (Pergamon Press, Oxford, 1975).
- [52] O. Bleu, G. Malpuech, and D. D. Solnyshkov, *Nat. Commun.* **9**, 3991 (2018).
- [53] J. Gea-Banacloche, Y.-q. Li, S.-z. Jin, and M. Xiao, *Phys. Rev. A* **51**, 576 (1995).
- [54] Y.-q. Li and M. Xiao, *Phys. Rev. A* **51**, R2703 (1995).
- [55] Z. Zhang, X. Liu, D. Zhang, J. Sheng, Y. Zhang, Y. Zhang, and M. Xiao, *Phys. Rev. A* **97**, 013603 (2018).
- [56] Y. Zhang, Z. Wu, M. R. Belic, H. Zheng, Z. Wang, M. Xiao, and Y. Zhang, *Laser Photonics Rev.* **9**, 331 (2015).
- [57] C. Eckart and B. L. Griffing, *Phys. Rev.* **50**, 1145 (1936).
- [58] M.-C. Chang and Q. Niu, *J. Phys. Condens. Matter* **20**, 193202 (2008).
- [59] D. Xiao, M.-C. Chang, and Q. Niu, *Rev. Mod. Phys.* **82**, 1959 (2010).
- [60] P. Ao and D. J. Thouless, *Phys. Rev. Lett.* **70**, 2158 (1993).
- [61] D. J. Thouless, P. Ao, and Q. Niu, *Phys. Rev. Lett.* **76**, 3758 (1996).
- [62] W. F. Vinen, *Nature (London)* **181**, 1524 (1958).
- [63] E. Madelung, *Z. Phys.* **40**, 322 (1927).
- [64] H. Kleinert, *Multivalued Fields: In Condensed Matter, Electromagnetism, and Gravitation* (World Scientific, Singapore, 2008).
- [65] G. Indebetouw, *J. Mod. Opt.* **40**, 73 (1993).
- [66] H. Sigurdsson, O. A. Egorov, X. Ma, I. A. Shelykh, and T. C. H. Liew, *Phys. Rev. B* **90**, 014504 (2014).
- [67] L. Dominici, R. Carretero-Gonzalez, A. Gianfrate, J. Cuevas-Maraver, A. S. Rodrigues, D. J. Frantzeskakis, G. Lerario, D. Ballarini, M. De Giorgi, G. Gigli *et al.*, *Nat. Commun.* **9**, 1467 (2018).
- [68] K. Schwab, N. Bruckner, and R. E. Packard, *Nature (London)* **386**, 585 (1997).
- [69] S. Eckel, J. G. Lee, F. Jendrzejewski, N. Murray, C. W. Clark, C. J. Lobb, W. D. Phillips, M. Edwards, and G. K. Campbell, *Nature (London)* **506**, 200 (2014).